NOTES AND CORRESPONDENCE

Observing Coherent Boundary Layer Motions Using Remote Sensing and Surface Pressure Measurement

WENSHOU TIAN, DOUGLAS J. PARKER, STEPHEN MOBBS, AND MARTIN HILL

Institute for Atmospheric Science, School of the Environment, University of Leeds, Leeds, United Kingdom

CHARLES A. D. KILBURN AND DARCY LADD

Rutherford Appleton Laboratory, Chilton, Didcot, Oxfordshire, United Kingdom

26 November 2003 and 14 April 2004

ABSTRACT

In this paper, high-frequency pressure time series measured by microbarographs are used to extract information on the existence and characteristics of convective rolls in the convective boundary layer. Rolls are identified in radar and satellite data, and it is shown that the pressure signals associated with the rolls have been detected in an array of microbarographs. The methodology of obtaining further information on roll characteristics from the array, notably orientation and drift velocity, is discussed in some detail. It is shown that the pressure time series contain signals representing the roll motion, approximately normal to the mean wind, and signals representing turbulent structures that drift along the mean wind direction. As the along-wind signals may dominate the time series, care is needed to identify the roll motion. Filtering of the higher-frequency along-wind signals can isolate the roll motion details. Also, a new approach using ''beam-steering diagrams'' to discriminate rolls from gravity waves and turbulent eddies is tested in both a numerical model and an observational case. In the beam-steering diagram, multiple centers of signal cross correlation can be used to identify different features in a single set of time series from an array of stations. The observations and model show that an array of microbarographs are able to resolve rolls if they are properly distributed with their spacing being tuned according to roll wavelength.

1. Introduction

It is known that the disturbances in the sheared convective boundary layer (CBL) are commonly organized into coherent motions such as convective rolls and Kelvin–Helmholtz billows, which are generally not easy to observe by direct means.

Under fair weather conditions, radar is a primary tool to detect roll circulations, while the existence of cloud streets in photometry and satellite imagery is a secondary indicator of roll circulations if the atmosphere is conducive to clouds. LeMone (1973) also used tower and aircraft data to document rolls.

Interpretation of radar pictures is complicated by the fact that they may sometimes exhibit roll-like structures that could be related to short gravity waves or Kelvin–Helmholtz billows rather than convective rolls. Weckwerth et al. (1997) found that in some cases the scales of convection are too small for radar to resolve the roll features. Although satellite images can show clearly whether cloud streets exist, the time at which roll circulations corresponding to those cloud streets begin to form cannot be inferred exactly from satellite imagery because of the intermittency of images. Meanwhile, cloud streets can be present but not appear in the satellite image when the CBL is too shallow to support cloud formation. On the other hand, not all cloud lines result from roll circulations; some of them may be caused by gravity waves (Worthington et al. 2001).

In consequence, an integrated study of those coherent structures needs not only radar and satellite imagery but other sources of data, which can be observed by affordable means, to infer roll information. Nappo et al. (2001) have used surface pressure perturbations measured by six microbarographs to detect gravity wave signals and their interaction with turbulence. Their preliminary results showed that a microbarograph network could be used to detect gravity waves, but they noted that uncertainties may exist. A study is undertaken here to examine convective rolls in the CBL, using radar

Corresponding author address: Dr. Wenshou Tian, Institute for Atmospheric Science, School of the Environment, University of Leeds, Leeds LS2 9JT, United Kingdom.
E-mail: wenshou@env.leeds.ac.uk

images and high-frequency pressure measurements collected by microbarographs. We attempt to clarify whether it is feasible to measure convective rolls by an array of microbarographs, and what kind of roll information could be gained from high-frequency pressure time series when convective rolls exist in the CBL. Wilson et al. (1992) have given an observational case in which horizontal rolls and the sea-breeze-induced convergence line together were found to contribute to initializing a deep storm. Therefore, observing the development and motion of rolls would have some value in storm initiation studies. If the roll emergence and roll motion could be inferred from pressure perturbations induced by roll circulations, a microbarograph network could be used to supplement detection of convective roll properties by the national radar network. This would be of value in locations distant from the radars and at times when the radars are not able to resolve the roll signals.

2. Observational dataset

The Chilbolton 3-GHz multiparameter radar is located approximately 80 km north of the south coast of England. More details about the radar can be found in Tian et al. (2003). The radar observations were made under fair weather conditions during a period of 18 days between 14 June and 31 October 2001. Three microbarographs, which were located near the Chilbolton radar (Fig. 1), collected continuous pressure time series dated from 14 August to 31 October 2001. One can note from Fig. 1 that microbarographs 1 and 3 are only 100 m apart and quite near to the radar. Barograph 2 is about 500 m away from barographs 1 and 3. This array pattern is not ideal but was constrained by available facilities (power and shelter) for the instruments. Hereafter, the time series measured by these three barographs are referred to as B1, B2, and B3.

The barographs measure the difference between the current atmospheric pressure and that of a temperature-maintained internal reference volume. The internal sensor has a full-scale range of 1 hPa, and an accuracy of 0.01 hPa can be reached. All the barographs have nominally identical sensors with the same specification (noise level, sensitivity, hysteresis, etc.). As we are only looking for differences in the pressure signal between the various sites, the absolute pressure reading is of little importance. However, for the purpose of calibration, some data were gathered with three barographs located in the same place using the same static sensor to find systematic gains going between three barographs.

Sounding profiles from the Larkhill radiosonde station, which is located about 25 km from Chilbolton radar, will be used to identify background flow patterns for the various cases considered. Satellite imagery is also used to confirm that roll circulations exist for the cases checked.

The original pressure time series have a sampling frequency of 1 Hz. In many cases, those daily time series

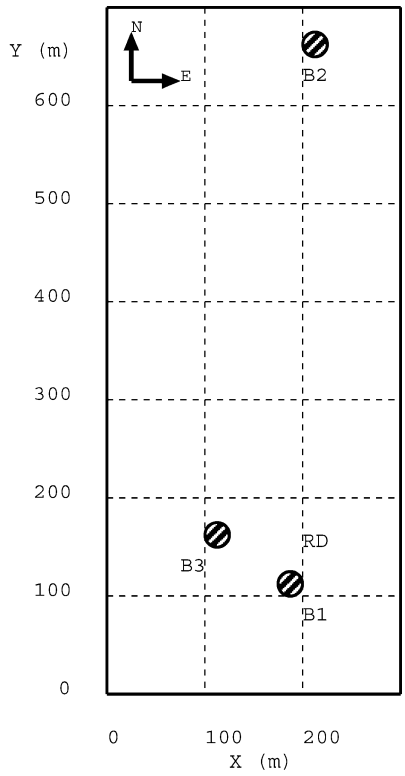

FIG. 1. The relative locations of three microbarographs, represented by B1, B2, and B3. The location of the radar is marked by RD.

are first Fourier transformed and then filtered with a Butterworth filter to obtain the signals of a specific frequency range. In the following, the analysis of the pressure will be based on various filtered time series. Since we are interested in the signals with periods less than 1 h, a Butterworth low-pass filter was first applied to the original daily pressure time series with a cutoff frequency of 1.0 h^{-1}. The process of such filtering is necessary for detrending time series and avoiding red noise before we focus on true signals of interest.

An nth-order low-pass Butterworth filter $f(\omega)$ is defined as

$$f(\omega) = \frac{1}{1 + \left(\frac{\omega}{\omega_0}\right)^{2n}}, \tag{1}$$

where ω is the frequency in cycles per time period $\mathcal{T}$ ($\mathcal{T}$ is also referred as data window), and ω_0 is called cutoff frequency. When $\omega < \omega_0$, this Butterworth low-pass spectrum is about unity. Similarly, a Butterworth bandpass filter is defined as

$$f(\omega) = \frac{1}{1 + \left(\frac{\omega - \omega_c}{\omega_0}\right)^{2n}}, \tag{2}$$

where ω_c is the center frequency.

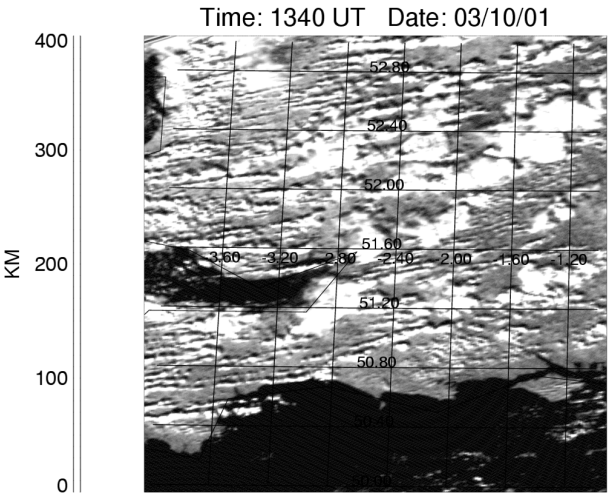

FIG. 2. The satellite image at 1340 UTC 3 Oct 2001.

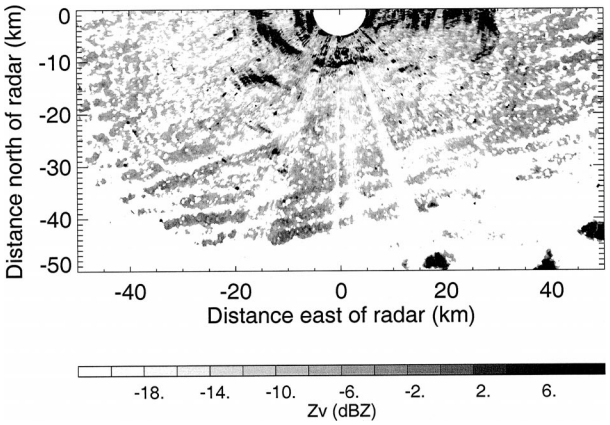

FIG. 3. The radar reflectivity in the horizontal plane at 1015 UTC 3 Oct 2001. The scan elevation was 1°.

3. Detection of roll signals from observations

Convective rolls are quite evident on the satellite image at 1340 UTC 3 October 2001 (Fig. 2). The radar began operating at 0823 UTC on this day and patches of roll structure can be noted from radar images from 0910 to 1200 UTC. Figure 3 gives the radar picture at 1015 UTC. Note that well-defined lines, aligned 60° from north, are evident. Both satellite images and radar pictures suggest that roll circulation is the dominant CBL flow pattern over the radar area from 1000 to 1200 UTC on this day.

Figure 4 shows the radar reflectivity in vertical planes at different times. At 0922 UTC, the CBL is shallow with an average height of 500 m, and there is no obvious up–down structure within the CBL. By 1029 and 1135 UTC, the CBL has become much deeper, with a height ranging from about 1000 m at 1029 UTC to 2000 m at 1135 UTC, and evident up–down structures can be noted

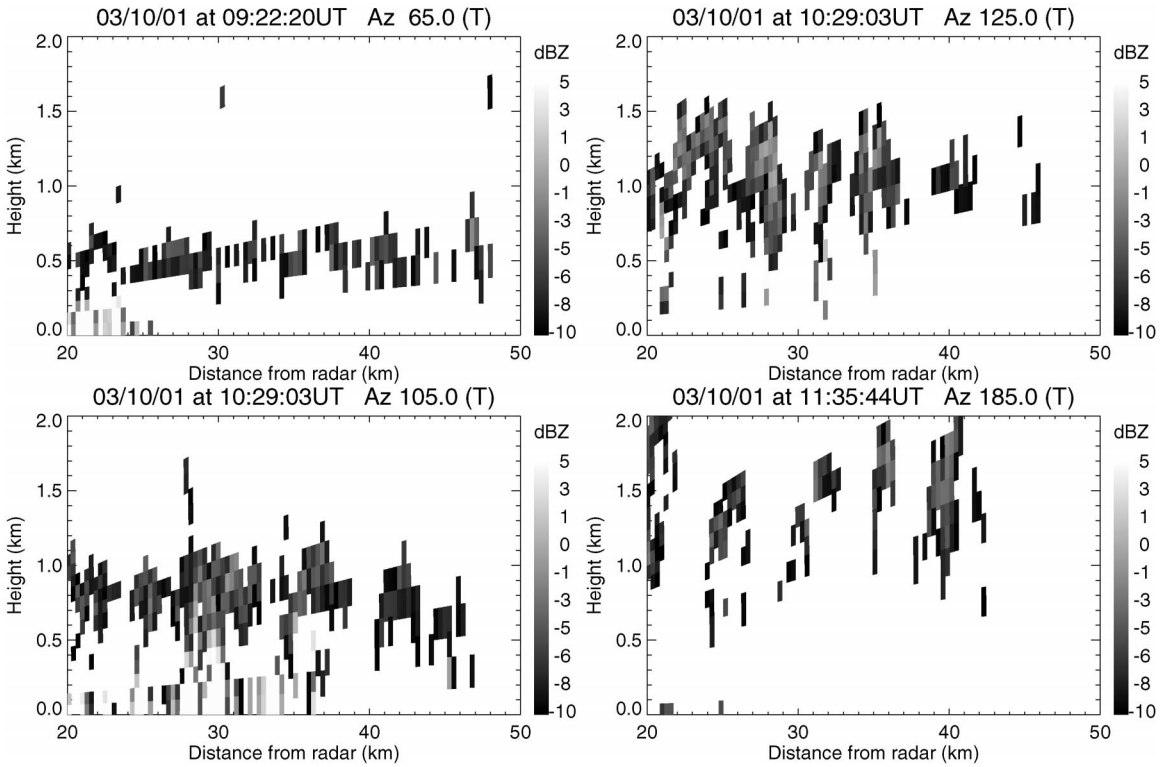

FIG. 4. The radar reflectivity in a vertical plane at different times. The upper dark envelope may represent the CBL top, while up and down structures may suggest the existence of rolls.

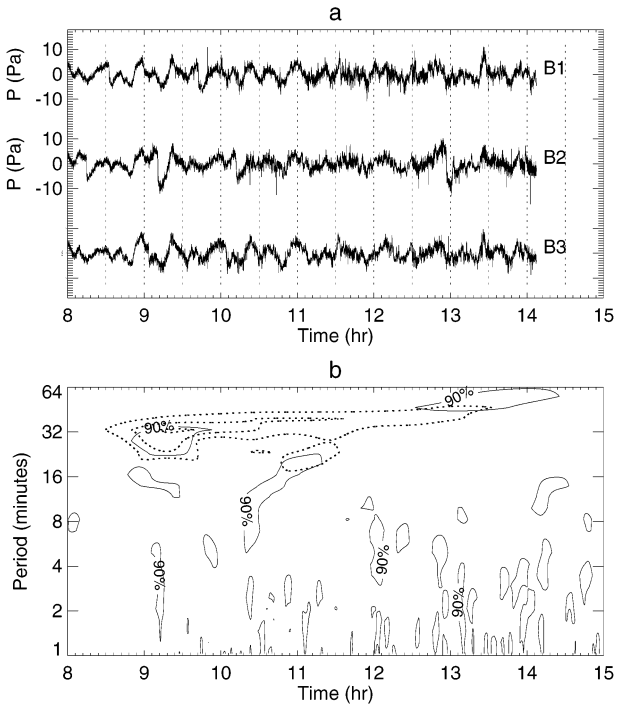

FIG. 5. (a) The low-pass-filtered time series (B1, B2, and B3) from 0800 to 1500 UTC and (b) wavelet analysis diagram of the series B3: dotted contour lines are for wavelet power; the significance of the power is tested by the global wavelet spectrum, and regions with 90% significant level are covered by solid lines.

within the CBL. Those up–down thermals suggest the dominance of roll circulations.

To detect roll signals from our high-frequency time series, wavelet analysis, which is thought to be a robust tool for identifying wavelike disturbances and for separating the events of interest from undesired processes (e.g., Farge 1992; Hauf et al. 1996), is first exploited. The wavelet analysis in this study is based on the program of Torrence and Compo (1998), and the wavelet power spectrum is tested against the global wavelet spectrum at 90% significant level.

Although there are local differences between the three time series from 0800 to 1500 UTC, the coherence is evident in Fig. 5a. The wavelet analysis diagram (Fig. 5b) indicates that there are significant wavelike events from 0830 to 1430 UTC. One event with its dominant period increasing gradually from about 6 to 16 min can be noted from 1030 to 1130 UTC. This event is most likely related to coherent convective eddies: the increase in the period is consistent with the increase of the CBL depth.

Also noticeable in Fig. 5 is the event with a dominant period around 30 min. Although this event is not statistically significant at 90% level from 1000 to 1300 UTC, it has a relatively large wavelet power. Note that the high-energy-content mode around 0900 UTC with a period of 30 min may have a wave nature, while the mode from 0930 to 1300 UTC is more like roll signals. Recall that roll signals can be noted on the radar pictures from 0910 to 1200 UTC.

From these observations, we conclude that the microbarograph data are indeed able to measure convective roll signals. However, without other information, it is apparent that the physical nature of signals (whether rolls, gravity waves, or other coherent features) detected by wavelet analysis cannot be confirmed by Fig. 5b only. To discriminate between gravity waves and convective rolls, the pattern velocity **C**, estimated from a time series, is helpful to understand the true nature of coherent modes (e.g., Hauf et al. 1996). On computing the velocity vector we wish to associate this with particular coherent patterns of motion. In particular, we attempt to distinguish the signals of gravity waves and convective rolls.

4. Determination of roll motion

For pure gravity waves the propagation speed C is related to the mean wind speed U through

$$C = U + C_{\text{int}}, \tag{3}$$

where C_{int} is the intrinsic gravity wave phase speed. Generally, the propagating speed of gravity waves C should be significantly different from the mean wind speed U; that is, $C \neq U$.

In the case of convective rolls, theoretical (e.g., Brown 1972) and observational (e.g., LeMone 1973; Weckwerth et al. 1999) studies have shown that the rolls are aligned close to the low-level geostrophic wind direction and to the mean wind in the boundary layer. The roll motion vector is then expected to be at right angles to the mean CBL wind and has been found in practice to be a fraction around 10%–20% of the boundary layer mean wind (Kelly 1984). In contrast, for gravity waves, the propagation characteristics of which are determined by the deep tropospheric profiles of wind and stability, the orientation is not, in general, constrained by the low-level wind direction.

A common method to determine the propagation velocity of a wavelike mode is the beam-steering approach (e.g., Zhou et al. 1984; Hauf et al. 1996), which is based on cross-correlation analysis. A minimum of three time series from different stations are required in this method; however, more stations will give more reliable information on signal propagation.

Assuming that a plane wave structure preserves its shape while passing over an observing network then, two time series of pressure p gathered at two stations will differ only by a time shift τ_{jk}, which is calculated from

$$\tau_{jk} = \mathbf{s} \cdot (\mathbf{r}_j - \mathbf{r}_k), \tag{4}$$

where $\mathbf{r}_j$ and $\mathbf{r}_k$ are position vectors of stations j and k, respectively, and can be determined from the network geometry, and $\mathbf{s}$ is the so-called slowness vector, which is related to the propagation velocity vector **C** through

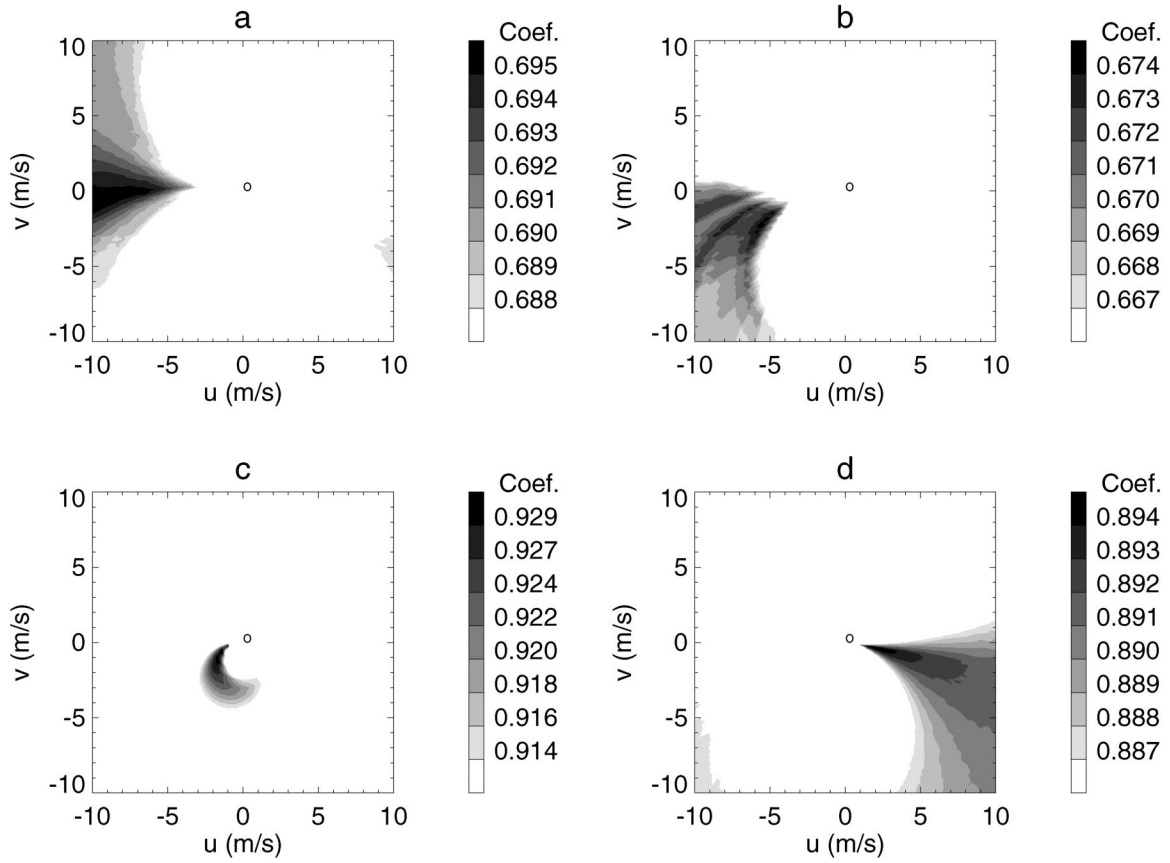

FIG. 6. The beam-steering diagrams for the time series (a), (c) 0830–1030 UTC and (b), (d) 1030–1230 UTC: (a), (b) low-pass-filtered time series; (c), (d) bandpass-filtered time series.

$$\mathbf{s} = \frac{\mathbf{C}}{C^2}. \tag{5}$$

In the beam-steering method, the desired phase velocity vector and slowness vector are given direction and magnitude, which are then varied over certain ranges. For a given sample of slowness vectors (directly related to feature propagation velocities) we effectively compute a cross-correlation function. This function is maximized when the test slowness vector corresponds to that of real propagating features.

For a test phase speed and propagation direction, the corresponding phase shifts, $\tau_{jk}(\mathbf{s})$, due to the observation network geometry are calculated from (4). Cross-correlation functions at time lags $\tau_{jk}(\mathbf{s})$ are calculated correspondingly between all pairs of time series, and a parameter C_r, can be constructed from the summation of $C_{jk}[\tau_{ij}(\mathbf{s})]$ (Hauf et al. 1996):

$$C_r[\tau_{ij}(\mathbf{s})] = \frac{2}{N_s(N_s - 1)} \sum_{j>k}^{N_s} C_{jk}[\tau_{ij}(\mathbf{s})], \tag{6}$$

where C_{jk} is the standard cross-correlation function between two series. Finally, the true phase velocity is the one with which the estimated C_r, at the time shift $\tau_{jk}(\mathbf{s})$ is the largest among all given slowness vectors.

It should be realized that the pure two-dimensional structures may be disrupted by three-dimensional turbulent eddies. These eddies drift with the mean wind and lead to motion vectors maximizing the cross-correlation function close to the mean wind vector. As a result, there are several maxima of the cross-correlation function that are possible: eddies provide a maximum close to the mean wind, rolls give a maximum normal to the mean wind and with lower amplitude, and gravity waves give a maximum that may differ from each of these. Here, we display these in a ''beam-steering diagram'' of the cross-correlation function plotted in the velocity plane.

Considering once more the observations from 3 October 2001, the beam-steering diagrams for two time periods, 0830–1030 and 1030–1230 UTC, are shown in Fig. 6. If the time series are low-pass filtered with a cutoff frequency of 1.0 h^{-1}, the corresponding beam-steering diagrams for both time periods (Figs. 6a,b) show only one maximum center, although the phase speed and direction are different for those two time periods (see Table 1). The estimated phase speed and drift direction within the time period 0830–1030 UTC are close to the observed CBL mean wind at 1400 UTC. The phase speeds within the time periods 1030–1230

TABLE 1. The phase speed C and phase direction C_d estimated from the beam-steering method using the time series for three different time periods: 0830–1030, 1030–1230, and 1300–1500 UTC. Subscripts l and b denote low-pass- and bandpass-filtered time series, respectively. The observed wind vectors from sounding profiles at 1400 UTC are also listed [U_{max} and U_{mean} are maximum and mean wind speeds between the surface and 750 hPa (the CBL top), respectively; U_{md} and U_{nd} are their corresponding directions.]

Time (UTC)	0830–1030	1030–1230	1300–1500	1400
C_l (m s^{-1})	10.5	6.0	5.5	12.9 (U_{max})
C_{dl} (°)	265.0	247.0	246.0	260.0 (U_{md})
C_b (m s^{-1})	1.5	2.0	5.5	11.1 (U_{mean})
C_{db} (°)	248.0	99.0	109.0	253.8 (U_{nd})

and 1300–1500 UTC are only about half of the CBL mean wind speed, although the phase directions are not very different. One can note that the peaks in the correlation function are along the direction of the mean wind, consistent with signals corresponding to convective eddies moving downwind. There is no simple evidence in Figs. 6a and 6b of cross-wind signal, which would be an indicator of roll motion.

From Eq. (6) it is possible to show that the pattern that would appear in a beam-steering diagram based on two stations observing a perfect two-dimensional signal would be a family of circles of increasing radius, with the true propagation velocity lying on the smallest. Since our network consists of two pairs of stations that are effectively coincident and a third pair (B1, B3) that are too close to resolve the long wave rolls, the beam-steering diagrams are dominated by such arclike patterns. Also, the pattern is dominated by the downwind-drifting features and the cross-wind signal is not detectable above this dominant pattern. Note that Fig. 6a shows a single maximum that corresponds to a large phase speed, implying that pressure signals in the earlier stage of boundary layer evolution are strong and fast moving. In the mature stage from 1030 to 1230 UTC, Fig. 6b contains multiple maxima, consistent with the theoretical signal from a two-station array as discussed above.

To overcome this network deficiency, the time series are bandpass filtered with a center period 0.5 h. Under such circumstances, fast-moving turbulent eddies are filtered out and the beam-steering diagram should be able to resolve cross-wind signals. Figure 6d indicates that there is indeed a cross-wind phase velocity within the time period 1030–1230 UTC. However, there is no cross-wind vector for the time period 0830–1030 UTC. The corresponding beam-steering diagrams for 1300–1500 UTC have similar features as those for 1030–1230 UTC, except that the cross-wind speed from 1300 to 1500 UTC is about twice as large as that from 1030 to 1230 UTC. Although (due to the inadequacy of our network) the exact moving speeds are not resolved, the results here indicate that the event from 0800 to 1000 UTC consists of a gravity wave signal rather than rolls, while the event from 1000 to 1500 UTC is roll signals.

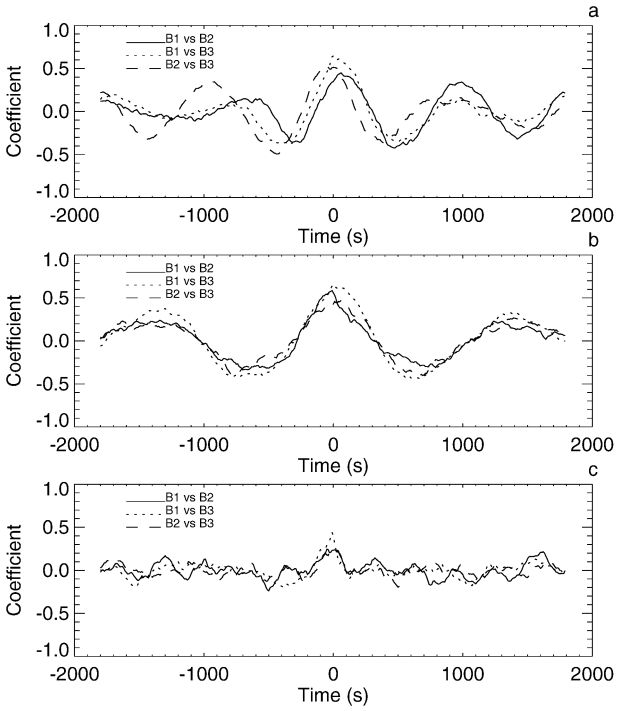

FIG. 7. Cross-correlations calculated from low-pass-filtered time series (cutoff period is 0.5 h) within three different time periods: (a) 1000–1100, (b) 1100–1200, and (c) 1200–1300 UTC.

Figure 7 gives cross-correlation coefficients between the low-pass-filtered (cutoff period is 0.5 h) time series within different time periods. The correlations change dramatically from 1000 to 1300 UTC, both in magnitudes and coherent patterns. From 1000 to 1100 UTC (Fig. 7a), there are significant time shifts between correlation patterns of different pairs of time series: the center peak of those cross-correlation functions is positive for B1–B2 and negative for B2–B3, since the separation vectors of those points are almost equal and opposite. A predominant period of around 15 min could also be detected in those coherent patterns. The coherent period increases further to about 20 min within the time period 1100–1200 UTC, but the phase differences become smaller (Fig. 7b). This relatively long period is consistent with the relatively slow drift of rolls across the mean wind direction. Note that the short time-lag cross correlations are probably dominated by 3D eddies, and the characteristic lags are wider if the time series are bandpass filtered (not shown). After 1200 UTC, coefficients and coherent periods become much smaller; however, phase differences can still be noted. It appears that roll circulations began to breakdown after 1200 UTC when convection was further intensified.

In summary, it seems that with the help of filtering we can separate the along-wind from the across-wind signal in the data, even from our inadequate observing network. As a result of the network configuration, there are no two slowness vectors that are perpendicular to

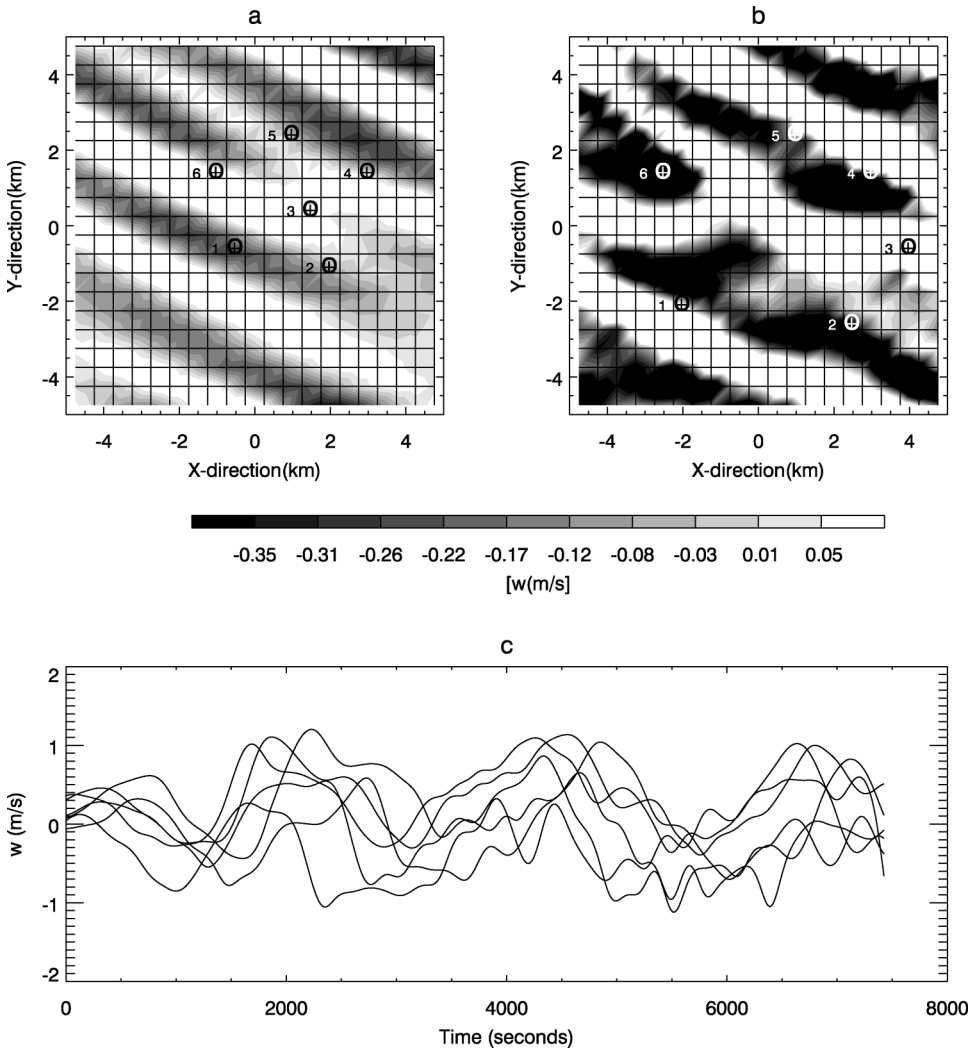

FIG. 8. The horizontal slices of the vertical velocity from two model realizations: (a) for the realization at the start of time series collection and (b) for the realization at the end of time series collection. (c) Six time series gathered at the points marked in (a) are shown for reference.

each other in these beam-steering diagrams of our observational case. To further clarify the feasibility of inferring roll motion from a proper observational network, an idealized study based on the model data is discussed in the next section.

5. An idealized study

Idealized roll circulations were generated by performing a numerical model simulation over a 10 km by 10 km flat domain with a horizontal grid spacing of 500 m. The model is based on the Met Office boundary layer model called Boundary Layer above Stationary, Inhomogeneous Uneven Surface (BLASIUS), in which a terrain-following coordinate system is employed to represent small-scale topography. The model is configured with a first-order turbulent scheme that is similar to that employed in large-eddy simulations (e.g., Deardorff 1974), except that the mixing length scale is arbitrarily chosen. The model is forced by a diurnal thermal forcing at the model's surface and a constant large-scale geostrophic wind of 11 m s^{-1} with a direction of 325°. More details about the numerical model and the model setup can be found in Tian et al. (2003). The model surface perturbation pressure field was gathered every 10 s for 2 h of simulation after roll circulations had been developed. Figure 8 shows two model realizations of the vertical velocity field at the 600-m model level. Rolls with an orientation of about 120° from north are evident and persistent throughout the time sequence examined. Figure 8c also shows six detrended time series gathered at six different points within the model domain, as indicated in Fig. 8a. One can note that wavelike features and phase differences between those time series are evident.

For a network with the minimum number of stations

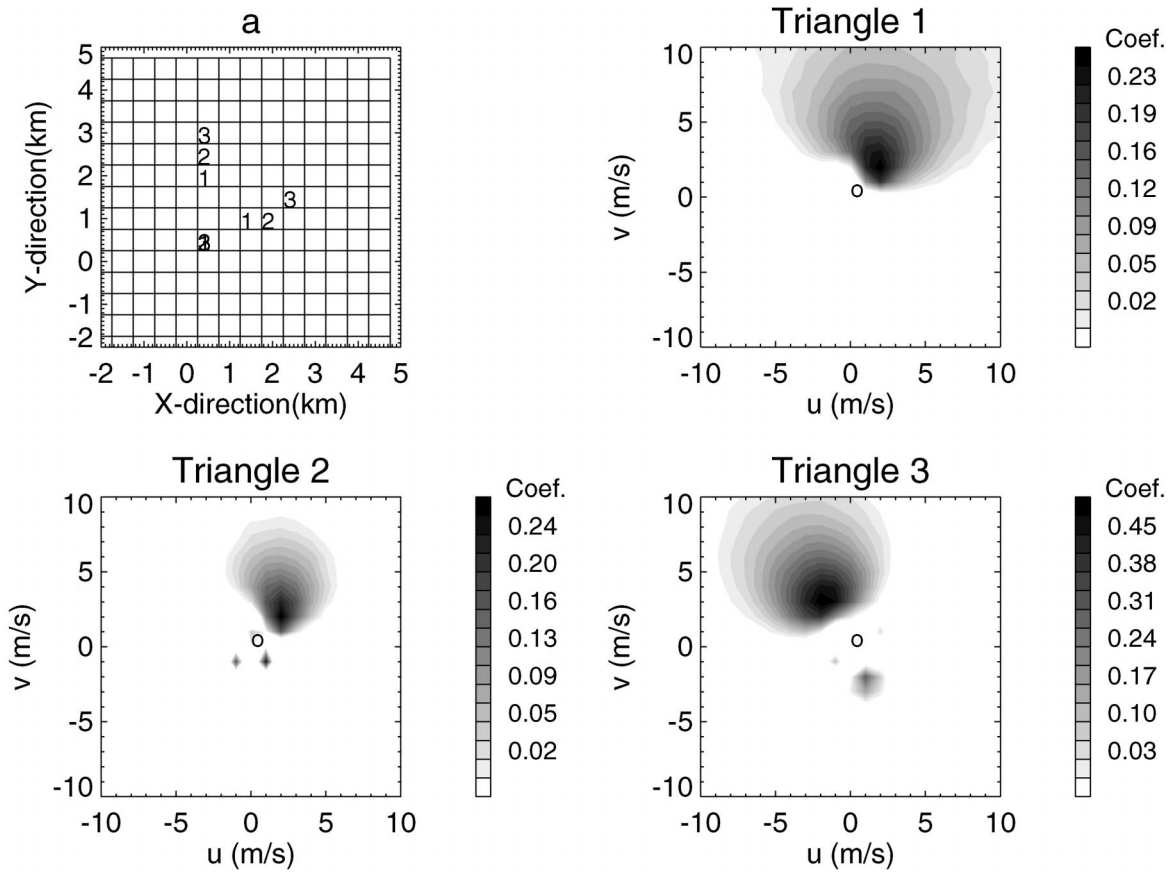

FIG. 9. The parameter C_r in the phase velocity space associated with three different triangles marked in (a). The three triangles are representive of three different networks. Note that the first point for the three triangles is at the same point.

(three) the optimum configuration to detect a moving pattern is an equilateral triangle with a spacing tuned to modes of the certain wavelength of interest (e.g., Briggs 1984). One can expect that an equilateral triangle with specific spacing should be suitable for time series that contain a single mode with a specific wavelength. For convective rolls, since we expect to capture signals in two different directions with different wavelength, an equilateral triangle may not always be suitable.

Figure 9 shows the beam-steering diagrams for three different triangles applied to the model data. Note that different triangles pick up different signals. Triangles 1 and 2 capture the cross-roll phase motion, while triangle 3 picks up along-roll motion. It is apparent that whether a triangle can pick up roll information depends on its spacing. When the spacing of the triangles is less than 1000 m and greater that 2500 m, the beam-steering diagrams fail to give sound information about the signal propagation. From the correlation point of view, the minimum spacing of the equilateral triangle is one-quarter of the signal wavelength and the maximum spacing equals the signal wavelength, which is about 3000 m in Fig. 8.

Again, no two vectors that are perpendicular to each other can be observed from Fig. 9. By analogy to radar techniques, the spacing of a network needs to be tuned for different modes with different wavelengths. One equilateral triangle has just one characteristic length scale and is therefore tuned to just one signal. If the turbulent eddies have a wavelength that is on the same order as that of cross-wind drifting rolls, it is possible to get characteristic roll features with an equilateral triangle network. Then, at this stage, one may expect that a wider array should be able to pick up different signals.

Six grid points, which are representive of an apparent network, are selected (see Figs. 8a,b), and hence, six pressure times series are obtained for beam-steering analysis. These model times series of pressure are filtered first for the purpose of detrending and getting rid of numerical noise.

The parameter C_r in the beam-steering method is first estimated based on the apparent network marked in Fig. 8a and displayed in Fig. 10a. There is only one significant maximum center in Fig. 10a, which corresponds to a phase speed of 7.6 m s^{-1} and a phase direction of 336.8° ± 5°. This phase velocity is quite close to the large-scale geostrophic wind used in the model simulation and may be associated with the coherent motion in the along-roll direction. However, another expected maximum center that should be associated with the

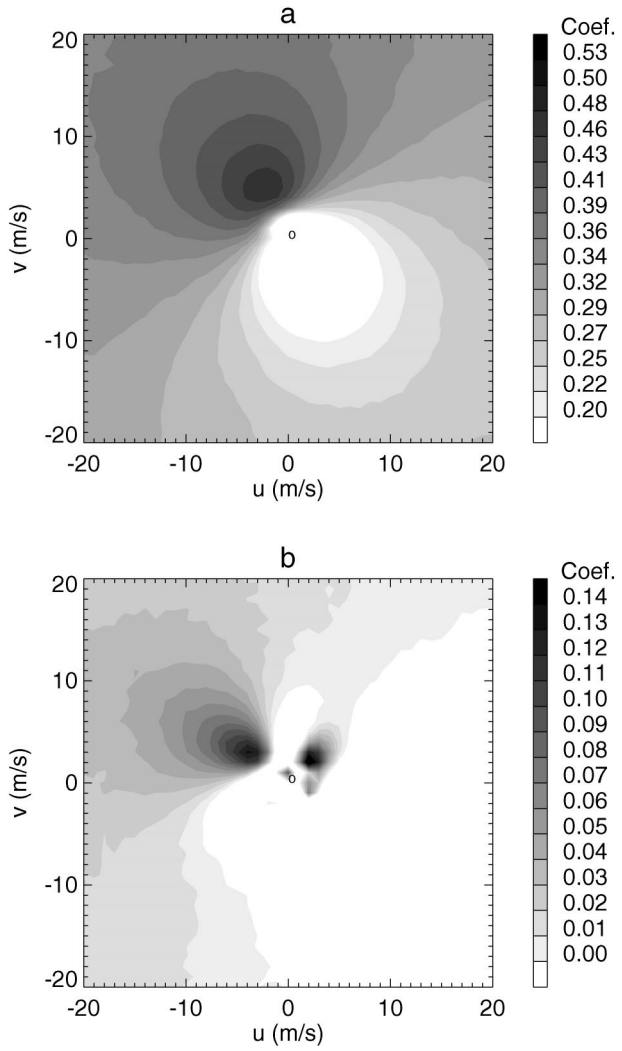

FIG. 10. The parameter C_r in the phase velocity space based on (a) the idealized network in Fig. 8a and (b) the network in Fig. 8b.

transverse velocity of rolls is not visible in Fig. 10a. If the network shown in Fig. 8b is used, the corresponding beam-steering diagram (Fig. 10b) exhibits a feature characteristic of roll circulations with two maximum centers pointing in two perpendicular directions. The results here suggest that a beam-steering diagram is sensitive to the network geometry regarding to the transverse velocity of rolls due to relatively weak coherence in the cross-roll direction.

6. Conclusions and remarks

Various data analysis techniques, including Fourier transform, filtering, wavelet analysis, cross-correlation analysis, and beam steering, have been used to extract useful information on convective rolls from pressure time series measured by microbarographs. The analysis of high-frequency pressure time series indicates that sensitive microbarographs can be used as an ancillary tool to detect coherent motions, including convective rolls in the planetary boundary layer. The roll information obtained from high-frequency pressure time series is useful for an integrated study of convective rolls.

Wavelet analysis can separate wavelike signals, but it is hard to confirm their physical nature. It is extremely difficult to discriminate between convective rolls and internal gravity waves, as well as the downwind drifting of turbulent eddies. A beam-steering diagram is found to be helpful for understanding the nature of coherent modes. The feature that rolls exhibit coherence in both roll direction and cross-roll direction while turbulent eddies may, at the most, exhibit some coherence along the mean wind direction in the boundary layer makes it possible to detect convective rolls using beam-steering analysis. The test based on idealized roll circulations obtained from a model simulation shows that the approach is indeed useful.

The beam-steering diagrams are sensitive to the network geometry as well as the signal wavelength under consideration. To obtain reasonable and desired results, the network should be properly distributed with spacing being tuned according to roll wavelength. An equilateral triangle is the theoretical optimal distribution for a three-point network. The minimum spacing is a quarter of the roll wavelength, while maximum spacing should equal the roll wavelength. To observe rolls, we have to be aware that rolls have two different wavelengths in two perpendicular directions. We have found that for a three-point network the signal in the beam-steering diagram is polluted by ''noise'' from nonroll turbulence, so that at least six stations were needed in our model data to resolve the rolls correctly. However, our results also indicate that with the help of filtering we can separate the along-wind from the across-wind signal in the data, even from our inadequate observing network. The key is filtering out the eddies smaller than rolls.

Acknowledgments. Satellite data are provided by NERC Satellite Receiving Station, Dundee University, Scotland. Radiosonde profiles were kindly supplied by the Met Office. Comments and suggestions from three anonymous reviewers have improved the clarity of the results.

REFERENCES

Briggs, B. H., 1984: The analysis of spaced sensor records by correlation techniques. *Handbook for MAP, Vol. 13,* SCOSTEP Secretariat, 166–186.

Brown, R. A., 1972: On the inflection point instability of a stratified Ekman boundary layer. *J. Atmos. Sci.,* **29,** 850–859.

Deardorff, J. W., 1974: Three-dimensional numerical study of the height and mean structure of the heated planetary boundary layer. *Bound.-Layer Meteor.,* **7,** 81–105.

Farge, M., 1992: Wavelet transform and their application to turbulence. *Annu. Rev. Fluid Mech.,* **24,** 395–457.

Hauf, T., U. Fink, J. Neiser, G. Bull, and J.-G. Stangenberg, 1996: A ground-based network for atmospheric pressure fluctuations. *J. Atmos. Oceanic Technol.,* **13,** 1001–1023.

Kelly, R. D., 1984: Horizontal roll and boundary-layer interrelationship observed over Lake Michigan. *J. Atmos. Sci.,* **41,** 1816–1826.

LeMone, M. A., 1973: The structure and dynamics of horizontal roll vortices in the planetary boundary layer. *J. Atmos. Sci.,* **30,** 1077–1091.

Nappo, C. J., E. Dumas, and D. Auble, cited 2001: Analysis of surface pressure perturbations during VTMX. *VTMX Workshop Presentations,* Salt Lake City, UT, U.S. DOE. [Available online at http://www.pnl.gov/vtmx/presentations2001.html.]

Tian, W.-S., D. J. Parker, and C. A. D. Kilburn, 2003: Observations and numerical simulation of atmospheric cellular convection over mesoscale topography. *Mon. Wea. Rev.,* **131,** 222–235.

Torrence, C., and G. P. Compo, 1998: A practical guide to wavelet analysis. *Bull. Amer. Meteor. Soc.,* **79,** 61–78.

Weckwerth, T. M., J. W. Wilson, R. M. Wakimoto, and N. A. Crook, 1997: Horizontal convective rolls: Determining the environmental conditions supporting their existence and characteristics. *Mon. Wea. Rev.,* **125,** 505–526.

——, T. W. Horst, and J. W. Wilson, 1999: An observational study of the evolution of horizontal convective rolls. *Mon. Wea. Rev.,* **127,** 2160–2179.

Wilson, J. W., G. B. Foote, N. A. Crook, J. C. Fankhauser, C. G. Wade, J. D. Tuttle, and C. K. Mueller, 1992: The role of boundary-layer convergence zones and horizontal rolls in the initiation of thunderstorms: A case study. *Mon. Wea. Rev.,* **120,** 1785–1815.

Worthington, R. M., A. Muschinski, and B. B. Balsley, 2001: Bias in mean vertical wind measured by VHF radars: Significance of radar location relative to mountains. *J. Atmos. Sci.,* **58,** 707–723.

Zhou, M.-Y., D. H. Lenschow, B. B. Stankov, L. C. Kaimal, and L. E. Gaynor, 1984: Wave and turbulence structure in a shallow baroclinic convective boundary layer and overlying inversion. *J. Atmos. Sci.,* **42,** 47–57.